IAU Colloquium 190 on Magnetic Cataclysmic Variables
ASP Conference Series, Vol. 315, 2004
Sonja Vrielmann & Mark Cropper, eds.

Can the propeller outflow from AE Aquarii be imaged directly?

Martin Still

NASA/Goddard Space Flight Center, Greenbelt MD 20771, USA and Universities Space Research Association

Keith Horne

School of Physics and Astronomy, University of St Andrews, St Andrews, Fife KY16 9SS, Scotland

Christian Knigge

Department of Physics and Astronomy, Southampton University, Southampton SO17 1BJ, England

Abstract. We calculate the Hα luminosity of an outflow nebula resulting from propeller action in AE Aqr. While the outflow is bright enough to be detected as an extended source, 1 arcsec across, it is dominated by the point-spread function (PSF) wings of the central object. By subtracting a PSF model from *HST* PC data we rule out the extreme models of high mass-loss rate combined with narrow-angle outflow, but more precise measurements are required to explore the propeller parameter space further.

1. Introduction

It has been suggested that the rapid spin-down of the white dwarf in AE Aqr is the result of a large fraction of accreting material accumulating enough angular momentum from the magnetic field outside the corotation radius to be ejected from the system (Wynn, King & Horne 1997). A large body of observations across the electromagnetic spectrum (see Pearson 2004 for a summary) reveal a wealth of peculiar phenomena which, while not explained satisfactorily by an accretion model, fit well into the propeller scenario. It has also been suggested that the propeller phase is a short-lived, but vital, stage in the evolution of a large number of magnetic cataclysmic variables (Schenker 2004), making AE Aqr a unique opportunity to understand a rare mode of accretion.

The propeller effect is seemingly an inevitable consequence of rapid white dwarf rotation in our models of stellar accretion. Gas in transit between the two stars is expected to be at least partially diamagnetic (King 1993) and provide some initial resistance to the magnetic field it is penetrating. However this resistivity is currently wrapped up into a single dimensionless parameter which we take on faith to be the right magnitude to drive a propeller. In reality the parameter is whitewashing physical processes that have yet to be quantified.

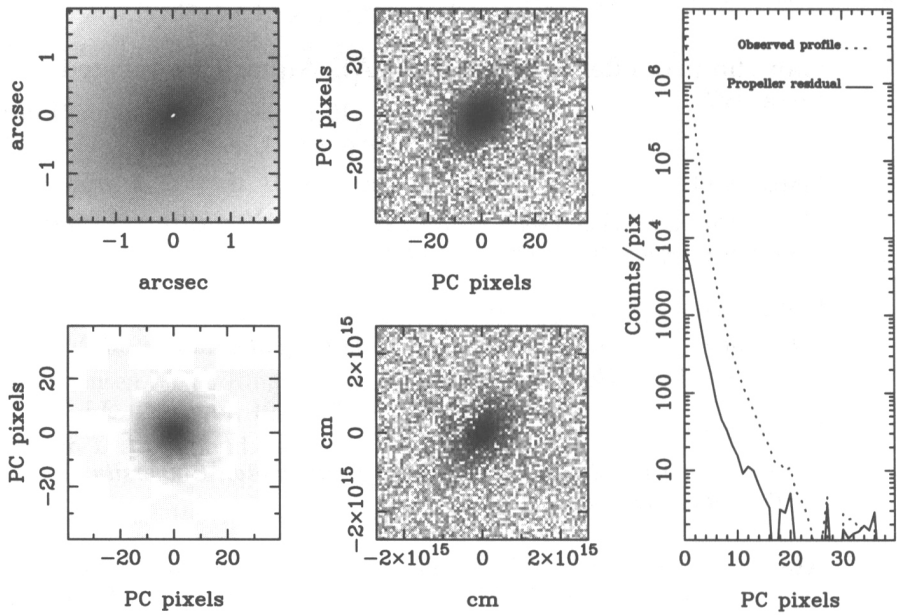

Figure 1. Model images and radial profiles of the propeller outflow. We simulate an *HST* PC Hα exposure of 100 sec duration. See text for a full description.

In response to this we ask whether there is an observational method to prove the existence of a propeller in this source. The ejected material expands through the interstellar medium, where we determine that the brightness of the outflowing gas is significant, while the size of the detectable region is several orders of magnitude smaller than any likely shell from a previous nova explosion. At the distance of AE Aqr (100 pc) this outflow would be detected easily with ground-based observatories were it not for the contaminating effect of the bright central point source. To detect the outflow it is imperative to be able to subtract the PSF of the central source accurately. The Planetary Camera (PC) on-board the Hubble Space Telescope (*HST*) provides a narrow PSF and fine spatial resolution, while minimizing background counts. Below we determine whether we can detect the outflow by carefully subtracting the central source from a PC image.

2. Predicted Hα nebula luminosity

An estimate of the brightness of the outflow nebula requires an understanding of its electron density as a function of distance from the source, $n_e(R)$. Wynn et al. (1997) argue that 10^{17-18} g s^{-1} of plasma is ejected from AE Aqr in a thin stream, with trajectories close to the orbital plane. Here will assume that the outflow is restricted initially to $\theta_{1/2} = \pm 10$ degrees about the plane. The outflow is inhomogeneous; each blob expands adiabatically where the initial thermal sound speed $c_s \sim 10$ km s^{-1}. Expansion velocities will increase by an

https://doi.org/10.1017/S0252921100002232 Published online by Cambridge University Press

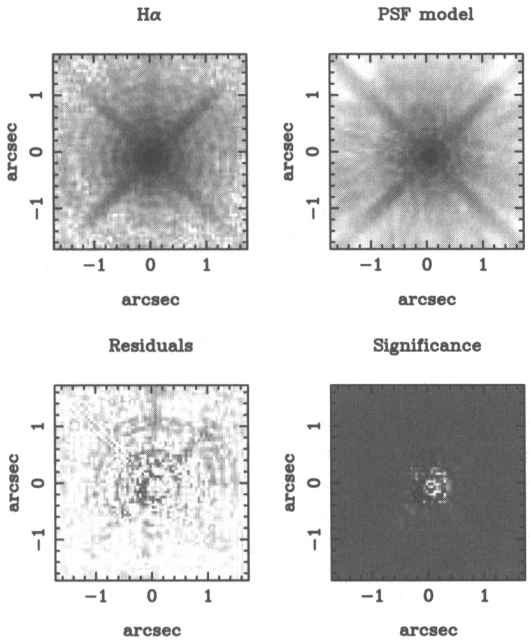

Figure 2. From top left to right left, the time-averaged Hα profile, a normalized PSF model, time-averaged residuals after subtracting the PSF model, and the significance of the residuals.

order of magnitude if they are involved in blob-blob collisions early in the dense, inner portion of the flow. Tomographic evidence (Wynn et al. 1997) suggests that ejection velocities $v_{\rm ej} \sin i \simeq 300$ km s^{-1}, where assume an inclination of $i \simeq 45$ degrees. Under these conditions, the outflow becomes fully homogeneous at $R_c \simeq 7 \times 10^{13}$ cm. AE Aqr is 100 pc distant; the size of a PC pixel at this distance is 1.5×10^{14} cm. Consequently initial blob sizes and densities are unimportant; we can assume that nebulosity observed by *HST* is smooth and the continuity equation is valid for describing the outflow:

$$n_e = \frac{X_e \dot{M}_{\rm ej}}{4\pi\theta_{1/2} R^2 v_{\rm ej} m_{\rm p}} \qquad (1)$$

$m_{\rm p}$ is the proton mass and X_e the electron ionization fraction. Blob-blob collisions will effect the gas in two ways. More collisions will move R_c closer to the source, while increasing the opening angle of the flow. This will effectively reduce n_e and, consequently, emission brightness.

The expansion timescale exceeds the recombination timescale when $R \gtrsim 10^{12}$ cm. Since the ionization fraction is frozen-in beyond this critical distance, we can use Eqn. 1 to calculate n_e, assuming a fully-ionized H plasma ($X_e = 1$). Outflow geometry yields an emission measure and brightness.

Assuming case B recombination, the Hα luminosity, $L_{\rm H\alpha}$, within an annulus of inner and outer radii R_1 and R_2, where R_1 is 1 pixel width from the source,

https://doi.org/10.1017/S0252921100002232 Published online by Cambridge University Press

is given by:

$$L_{\mathrm{H}\alpha} = 10^{29}\left(1-\frac{R_1/R_2}{0.5}\right)\left(\frac{\dot{M}_{\mathrm{ej}}}{10^{18}\mathrm{g/s}}\right)^{2}\left(\frac{\theta_{1/2}}{10^{\circ}}\right)^{-1}\left(\frac{v_{\mathrm{ej}}}{430\mathrm{km/s}}\right)^{-2}\left(\frac{R_1}{1.5\times10^{14}\mathrm{cm}}\right)^{-1}\mathrm{erg\,s^{-1}} \quad (2)$$

The predicted Hα image of the outflow is plotted in the top-left panel of Figure 1. The orbital inclination of the binary is assumed to be 45 degrees and the orientation on the sky is arbitrary. The center of the outflow, where the gas is blobby, has been omitted from the calculation. The same data are simulated over a 100 sec exposure through the *HST* PC Hα filter with Poisson noise added (top-right)PSF. A noise-added central point source, simulating the AE Aqr's intrinsic Hα and continuum emission, is added to the extended source at lower-left. A simple 2-dimensional Lorentzian, approximating, the size and shape of the PC PSF has been adopted. We can see that outflow emission is completely dominated by the star. Since the nebula has not been identified in previous images, this is as expected. However, by subtracting an accurate, scaled model of the PSF from the image (lower-right panel) we recover the extended emission.

Note however that the central pixel is saturated, providing scheduling problems. Dynamic range proved to be a challenge for this experiment. The point source is bright enough to saturate the CCD in just a few seconds, and the overheads associated with PC exposures make acquisition of a large number of unsaturated images inefficient, requiring over 100 HST orbits to build up signal-to-noise sufficient for robust detection of the nebula. Consequently we sacrificed the central pixels and the central PSF information for longer individual exposure times.

3. Observations

AE Aqr was monitored by the *HST* PC over 4 consecutive orbits, resulting in 42 individual observations and a total exposure time of 1.47 ksec, Individual exposures were of duration 20, 40 and 50 sec providing dynamical range in the wings of the images. 32 R band images were also taken, each of 0.4 sec to employ as a PSF template.

4. Results

We attempted three methods of PSF subtraction from the PC images. The first used a composite image of all the R band images to define a PSF. The second used a "difference" image generated from the variability in the 42 Hα exposures. The third used the *HST* "Tiny Tim" PSF models provided by the instrument scientists (Krist & Hook 2001). The first method proved untenable because of the intrinsic differences between the R and Hα filter PSFs at the limits of our sensitivity. Similar problems occur for the second method where the Hα variability occurs over a fraction of the filter response. Furthermore the source was only moderately variable, so statistics for the difference PSF were not as good as hoped. Below we present results for the third method where the PSF subtraction was the most successful.

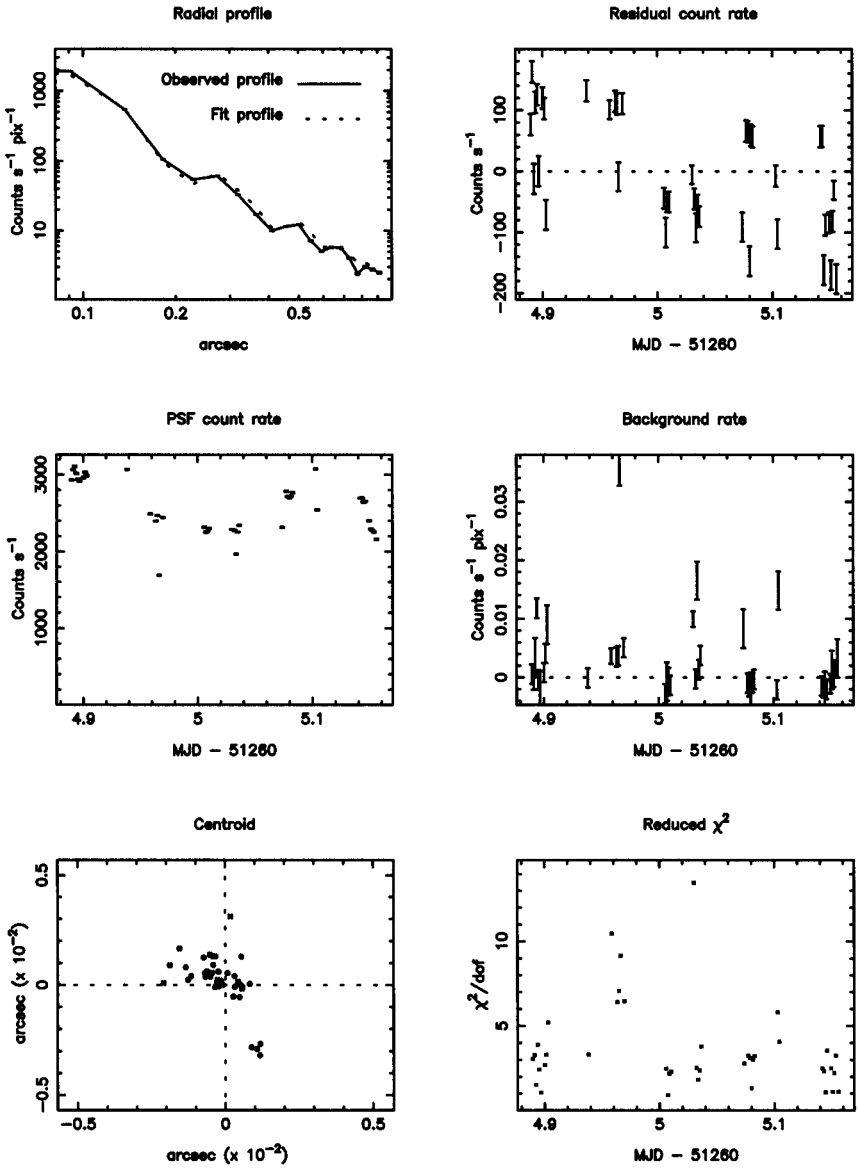

Figure 3. Best fit model parameters to the time-series of Hα images. From top left to bottom right we plot the spatial profile and PSF model fit averaged over azimuth and time, the residual count rates in the images after subtracting the PSF model, the PSF normalization, the background count rate, the PSF centroid and the χ^2 for each fit.

https://doi.org/10.1017/S0252921100002232 Published online by Cambridge University Press

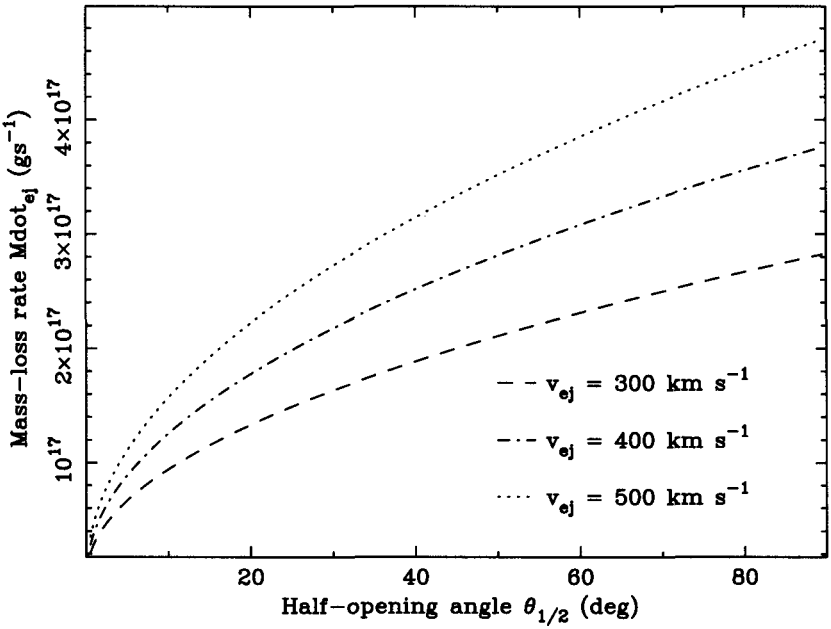

Figure 4. Upper limits to the mass loss rate, $\dot{M}_{\rm ej}$, as a function of half-opening angle, $\theta_{1/2}$, for three different outflow velocities $v_{\rm ej}$.

We fit the model PSF plus a spatially-constant background to each Hα image individually using least-squares deconvolution. The four most central pixels were saturated and ignored during the fit. In the top-left panel of Figure 2 we plot the mean of all Hα data where cosmic rays and chip cosmetics have been removed using a σ-clipping method during the fitting process. Unlike the simulation of Figure 1, we must rely on the PSF model to subtract the observed diffraction spikes and Airy fringes; the model PSF is displayed in the top-right panel. Note that there is some upward bleeding of electrons from the saturated pixels. We have made no attempt to remove this. The lower-left panel is the mean of all the residual images after the fitted model has been subtracted. The lower-right panel is the image of residuals normalized to the noise, σ, in each pixel. Black and white correspond to $\pm5\sigma$. While there is some residual structure in these images from uncertainties in the spike and fringe calibrations and chip bleeding, there is no significant extended emission that can be associated with an outflow.

Figure 3 plots the results from each individual fit. The top-left panel is the radial profile of the mean image and PSF model, averaged over time and azimuth. The top-right panel shows the residuals after subtracting the model. PSF normalizations are plotted in the middle-left panel, revealing the variability of the central source during the observations and the background level is presented middle-right. Lower-left provides the scatter in the PSF centroid across the fits and lower-right the χ^2 per degree of freedom.

https://doi.org/10.1017/S0252921100002232 Published online by Cambridge University Press

Limits can be placed on the outflow parameter space due to our non-detection of extended emission. However there is inconsistency between the scatter and the 1σ error bars of the fit residuals that requires tracking down. For now we will assume that the detection limit per exposure is 3σ relative to the residual error bars. Figure 4 presents upper limits to the binary mass-loss rate as a function of outflow half-opening angle for three values of outflow velocity. The data rule out only those models of high mass-loss rate and small opening angle. There is consequently plenty of scope in the future for deeper experiments.

5. Conclusions

The propeller model provides an elegant solution to a large number of exotic behaviours exhibited by AE Aqr. One approach to verify the existence of a propeller is to image the resulting outflow directly. While the non-detection provided by a moderately long set of *HST* exposures is initially disappointing, we have two reasons to remain optimistic. Firstly, the major point to take from this work is that there is a "good chance" that the outflow, if it exists, should be detectable by currently operating detectors. Second, the current data rules out only the extreme cases of mass loss rates, $> 10^{17}\,\mathrm{g\,s^{-1}}$, combined with small numbers of blob-blob collisions resulting in narrow, ~ 10 degree, half-opening outflow angles. A large fraction of the probable outflow parameter space remains to be explored with more sensitive observations.

References

King, A. R., 1993, MNRAS, 261, 144
Krist, J. & Hook, R., 2001, "The Tiny Tim Users' Guide" v.6
Pearson, K. J., 2004, this volume
Schenker, K., 2004, this volume
Wynn, G. A., King, A. R. & Horne, K., 1997, MNRAS, 286, 436

https://doi.org/10.1017/S0252921100002232 Published online by Cambridge University Press